# Using ion mobility spectrometry to understand signal dilution during tandem mass spectrometry sequencing of digital polymers: Experimental evidence of intramolecular cyclization

Isaure Sergent, Thibault Schutz, Jean-françois Lutz, Laurence Charles

Received: 25 April 2024 | Revised: 22 May 2024 | Accepted: 23 May 2024

DOI: 10.1002/rcm.9852

RESEARCH ARTICLE

Rapid Communications in Mass Spectrometry WILEY

# Using ion mobility spectrometry to understand signal dilution during tandem mass spectrometry sequencing of digital polymers: Experimental evidence of intramolecular cyclization

Isaure Sergent[1] | Thibault Schutz[2] | Jean-François Lutz[2] | Laurence Charles[1]

[1]Aix Marseille Université, CNRS, UMR7273, Institut de Chimie Radicalaire, Marseille, France

[2]Université de Strasbourg, CNRS, Institut de Science et d'Ingénierie Supramoléculaires (ISIS), Strasbourg, France

**Correspondence**
Laurence Charles, Aix Marseille Université, CNRS, UMR7273, Institut de Chimie Radicalaire, 13397 Marseille, Cedex 20, France.
Email: laurence.charles@univ-amu.fr

**Funding information**
Agence Nationale de la Recherche, Grant/Award Numbers: ANR-19-CE29-0015-01, ANR-19-CE29-0015-02

**Rationale:** Optimizing the structure of digital polymers is an efficient strategy to ensure their tandem mass spectrometry (MS/MS) readability. In block-truncated poly(phosphodiester)s, homolysis of C–ON bonds in long chains permits the release of smaller blocks amenable to sequencing. Yet the dissociation behavior of diradical blocks was observed to strongly depend on their charge state.

**Methods:** Polymers were ionized in negative mode electrospray and activated in-source so that blocks released as primary fragments can be investigated using ion mobility spectrometry (IMS) or sequenced in the post-IMS collision cell. Collision cross sections (CCS) were derived from arrival times using a calibration procedure developed for polyanions using the IMSCal software. A multistep protocol based on quantum methods and classical molecular dynamics was implemented for molecular modeling and calculation of theoretical CCS.

**Results:** Unlike their triply charged homologues, dissociation of diradical blocks at the 2– charge state produces additional fragments, with +1 *m/z* shift for those holding the nitroxide α-termination and −1 *m/z* for those containing the carbon-centered radical ω-end. These results suggest cyclization of these diradical species, followed by H$^{\bullet}$ transfer on activated reopening of this cycle. This assumption was validated using IMS resolution of the cyclic/linear isomers and supported by molecular modeling.

**Conclusions:** Combining IMS with molecular modeling provided new insights into how the charge state of digital blocks influences their dissociation. These results permit to define new guidelines to improve either ionization conditions or the structural design of these digital polymers for best MS/MS readability.

## 1 | INTRODUCTION

One of the major breakthroughs enabled by tandem mass spectrometry (MS/MS) is undoubtedly biopolymer sequencing, where the nature and relative location of building units can be determined by analyzing MS/MS data using specific fragmentation rules. As long as chains consist of building units of different masses and dissociate via backbone cleavages independently of their sequence, biopolymers such as peptides,[1] oligonucleotides,[2] or carboxydrates[3] exhibit typical MS/MS patterns that allow their sequence to be reconstructed. The same principle applies to synthetic polymers and is highly valued for end-group analysis[4] or to differentiate blocks from random

copolymers.[5–10] MS/MS has also become an important technique for digital polymers, not only to decipher their sequence but also to guide their structural design.[11] In contrast to biopolymers, digital polymers do not aim to fulfill any biological functions and, unlike classical synthetic polymers, their structure is not conceived to ensure specific macroscopic properties. Their main purpose is to store information intended to be read.[12,13] Messages can indeed be written in their backbone due to specific sequences of co-monomers defined as letters and, to date, MS/MS is the most efficient sequencing method to retrieve such molecularly encoded information.[14] In this context, their structure can be purposely optimized to achieve the full sequence coverage requested for error-free reading. This has been the strategy employed by our group to prepare digital chains of increasing length, up to a recent record of 440 bits stored in a single poly(phosphodiester) (PPDE) macromolecule and decoded using a routine mass spectrometer.[15] Digital PPDEs have been carefully engineered to undergo programmed fragmentations when subjected to collision-induced dissociation (CID) as gas-phase anions.[16] Briefly, alkoxyamine moieties that cleave at lower energy than any bonds in PDE co-monomers are distributed between each segment of eight repeating units (i.e., one byte of information). As a result, a first soft activation step permits to disassemble these block-truncated PPDEs (b-PPDE) into their constituting blocks: the first block retains the original α-termination and contains one carbon-centered radical at the ω-end, the last block retains the original ω-termination and has a nitroxide at the α-end, and inner blocks are diradical species. As the size of so-released 8-mers is far below the analytical limit of MS/MS, a second activation stage can be performed for their de novo sequencing based on fragments produced after phosphate bond cleavages in each repeat unit. To prevent mass coincidence of blocks with the same co-monomeric composition and to determine their position in the initial chain, the design of b-PPDEs also includes tags carrying a specific mass signature and attached to each block except the first one, the lack of tag also enabling mass distinction.

In the first b-PPDE generation, these tags were nucleosides because their commercial availability as phosphoramidite species conveniently suited the synthesis protocol.[17] They were placed at the right-hand side of the coded segment, and their close proximity with the carbon-centered radical in the ω-end of inner blocks led to undesired rearrangements during CID. Radical-driven reactions were identified to efficiently compete with phosphate bond cleavages, which resulted in the production of new abundant products together with very partial series of ω-containing fragments.[18] Although series of α-containing ions enabled the full coverage of the 0/1 sequence of these blocks, the presence of intense side products prevented automated decoding using our in-house-developed MS-DECODER software.[19] This problem was solved after structural optimization of the alkoxyamine linker, using a rigid aromatic moiety to prevent undesired backbiting radical reactions and so produce cleaner MS/MS data for accelerated automated sequencing.[20] To address the issue of atom economy of importance in the field of digital polymers, the most recent structural design of b-PPDEs does no longer involve the nucleoside tagging system. Instead, the alkoxyamine group and the mass tag are combined in a single phosphoramidite reagent.[21] Different alkoxyamines based on 2,2,6,6-tetramethylpiperidin-1-yl)oxyl (TEMPO) and decorated with one tag were prepared and enabled the synthesis of uniform digitally encoded b-PPDEs. With this most recent design (Scheme 1), released inner blocks have their T-tag placed at the left-hand side of the coded segment, that is, in the vicinity of the nitroxide α-end and far away from the more reactive carbon-centered radical ω-group. Yet the dissociation behavior of inner blocks was observed to depend on their charge state: CID of triply charged species produces the eight ion series expected from bond cleavage at each phosphate moiety, whereas additional fragment families were produced on activation of blocks at the 2– charge state. Although not preventing reliable sequencing of the blocks, this complicates MS/MS data and somehow contributes to fragment signal dilution. The present study aims at understanding this phenomenon to propose relevant solutions to prevent its occurrence.

## 2 | EXPERIMENTAL

### 2.1 | Chemicals

Water, methanol (MeOH), and acetonitrile (ACN) used to prepare solutions subjected to electrospray ionization (ESI) were obtained from SDS (Peypin, France). Formic acid was purchased from Sigma-Aldrich (St. Louis, MO). Orthophosphoric acid ($H_3PO_4$, 85%) was obtained from VWR International (Fontenay-sous-Bois, France). All chemicals were used as received without further purification. Block-truncated PPDEs were prepared according to synthesis protocols detailed in a recent paper.[21] For ESI-IMS (ion mobility spectrometry)-MS analysis, b-PPDE samples (few mg) were dissolved in $H_2O$–ACN (50:50, v/v) supplemented with 0.1% formic acid and further diluted (1:10, v/v) with MeOH.

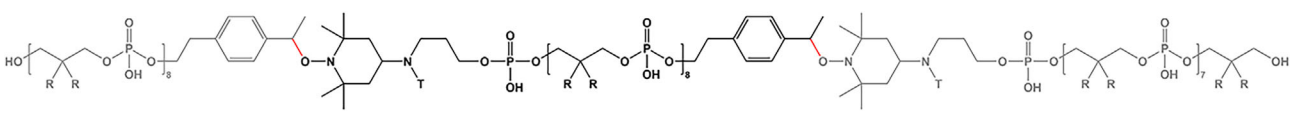

**SCHEME 1** Structure of a digital three-block PPDE, with R groups defining coding units (R = H for 0-bit, R = $CH_3$ for 1-bit); tags designated by T and alkoxyamine bonds in red. Initial and final blocks are in grey, whereas the inner block investigated in this study is in black. [Color figure can be viewed at wileyonlinelibrary.com]

## 2.2 | MS and IMS

High-resolution mass spectrometry and traveling wave ion mobility (TWIM) spectrometry experiments were all performed using a Synapt G2 HDMS instrument from Waters (Manchester, UK) operated in the negative ion mode (capillary ESI voltage, −2.27 kV; sampling cone voltage, −20 V; and extraction cone voltage, −6 V). The desolvation gas ($N_2$) flow was 100 L $h^{-1}$ at 35°C. A syringe pump was used to introduce sample solutions into the ESI source at a flow rate of 10 µL $min^{-1}$. In MS/MS experiments, deprotonated b-PPDEs were selected in the Q1 quadrupole and activated in the collision cell. For experiments performed on individual blocks, the cone voltage was adjusted between −60 and −80 V to induce in-source fragmentation of deprotonated b-PPDEs and produce blocks in the interface of the instrument. For pseudo-$MS^3$ sequencing, blocks were mass selected in the Q1 quadrupole and activated in the collision cell. For IMS-MS experiments, blocks were introduced (and eventually activated) in the ion trap device located in front of the TWIM cell and then ejected from the ion trap into a cooling cell (helium flow: 180 mL $min^{-1}$) before reaching the TWIM cell filled with $N_2$ (3.0 mbar) and operated in various wave height (WH, in V) and wave velocity (WV, in m $s^{-1}$) conditions. All activation stages used argon as the collision gas. Instrument control, data acquisition, and data processing of all experiments were achieved using the MassLynx (version 4.1) programs provided by Waters.

## 2.3 | Collision cross section calibration

Experimental arrival time distributions (ATD) of ions were extracted manually from MassLynx software, and arrival times ($t_A$) measured at peak apex were converted into experimental collision cross section (CCS) using IMSCal software.[22] Reference compounds were phosphoric acid clusters (1– and 2–) measured in He,[23] formed on ESI of a 2-mM solution in $H_2O$–ACN (50:50, v/v) and demonstrated in a recent study to enable good-quality CCS estimations for polyanions with no need for calibrants to match the chemical class of the analytes.[24] Throughout the text, CCS values are designated according to the nomenclature proposed by Pacholarz and Barran:[25] CCS experimentally determined in $N_2$ with TWIM calibrated with CCS reference in He was named $^{TW}CCS_{N2\rightarrow He}$. Therefore, experimental CCS values can be compared with $^{calc}CCS_{He}$ derived from three-dimensional (3D) molecular models.

## 2.4 | Molecular modeling and CCS calculation

A multistep protocol based on quantum methods and classical molecular dynamics (MD) was implemented. PPDE blocks were constructed, and protons were manually removed from the phosphate groups, assuming an even distribution of the two charges, that is, deprotonated sites located on phosphate groups 3 and 6 for 2– species.[26] Geometry optimization was performed at the semiempirical level with AMPAC (version 11 from SemichemInc., Shawnee, KS, USA) using the PM6 method.[27] Then, the restrained electrostatic potential (RESP) charges were calculated based on the Hartree–Fock method at the HF/6-31G(d) level using Gaussian16.[28] MD simulations of the doubly charged anions in vacuum were performed using GROMACS4.[29] These nonperiodic simulations were run over 100 ns (time step: 0.50 fs, 300 K, Berendsen thermostat), with no radial cutoffs for the nonbonded forces. Conformations were sampled every 1 ns from this trajectory. CCS values were calculated using the He-based trajectory method available in IMoS software[30] (default settings: 300 Pa). For PPDE blocks, $^{calc}CCS_{He}$ corresponds to the average value over the 100 sampled conformations. The GROMACS energy tool was used to extract the total energy from MD trajectory and reported values for most stable geometry of each isomer.

# 3 | RESULTS AND DISCUSSION

## 3.1 | Influence of charge state on CID pattern

As mentioned in Section 1, the structure of digital b-PPDEs is determined for a two-step reading methodology, the first one intending to release individual blocks from intact chains after cleavage of all alkoxyamine bonds and the second one aiming at sequencing each block.[17] That is, one $MS^2$ experiment is performed to deconstruct the b-PPDE, whereas multiple $MS^3$ experiments are required to analyze all blocks for their 0/1 sequence. To take advantage of the resolving capabilities provided by orthogonal acceleration time-of-flight (oa-TOF) mass analyzers to safely assign fragments, we use the same the Q-oa-TOF instrument for all steps. This means that the final sequencing steps are actually achieved according to pseudo-$MS^3$ experiments: deprotonated polymers are first activated in the instrument interface by increasing the cone voltage to induce their in-source dissociation; the so-released individual blocks can therefore be mass selected in the quadrupole for further excitation in the collision cell and measurement of their fragments in the oa-TOF.

In the negative ion mode, b-PPDEs readily ionize as deprotonated molecules, as shown in Figure 1A, with P1 chains detected with charge states ranging from 4– to 9–. For these digital polymers, the most stable gas-phase species are always observed to carry (3n – 2) negative charges, with n the total number of blocks. For example, the major signal observed for $[P1 - 7H]^{7-}$ at *m/z* 668.9 in Figure 1A is consistent with P1 being a triblock polymer. For the first activation stage, the simplest MS/MS data are obtained for precursor ions having their charge state equal to a multiple of the number of blocks. CID spectra are indeed more populated when deprotonated sites are not evenly distributed along the chains: as shown in Figure S1, blocks formed during MS/MS of $[P1 - 7H]^{7-}$ are all observed at two different charge states (2– and 3–). In contrast, an even distribution of deprotonated sites favors the release of individual blocks with the same single charge state in MS/MS. However, this holds true when

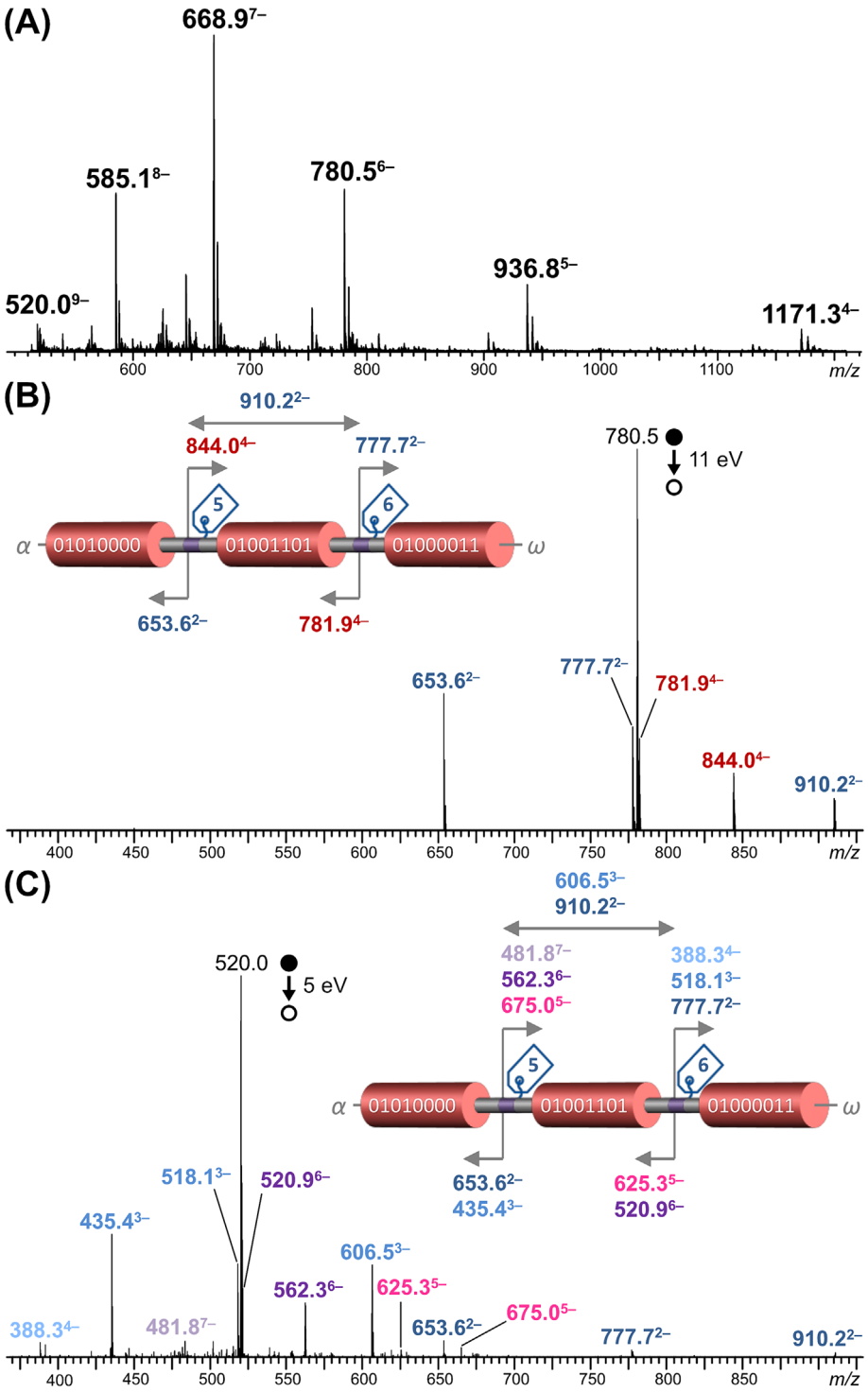


**FIGURE 1** (A) ESI(−)-MS of the triblock P1 polymer (4689.2 Da). MS/MS of (B) $[P1 - 6H]^{6-}$ at *m/z* 780.5 and (C) $[P1 - 9H]^{9-}$ at *m/z* 520.0, with dissociation schemes in inset. [Color figure can be viewed at wileyonlinelibrary.com]

the total number of negative charges remains low, as shown in Figure 1B, where the CID of $[P1 - 6H]^{6-}$ at *m/z* 780.5 produces all blocks at the 2− charge state (in blue). When released from $[P1 - 9H]^{9-}$ at *m/z* 520.0 (Figure 1C), individual blocks are mostly detected as $[Bi - 3H]^{3-}$ (at *m/z* 435.4 for B1, *m/z* 606.5 for B2, and *m/z* 518.1 for B3) but also at different deprotonation states. This is because the size of blocks is different depending on their location in the chain (Scheme 1), with the much shorter B1 tending to accommodate fewer charges than the other blocks. As a result, formation of $[B1 - 2H]^{2-}$ at *m/z* 653.6 on CID of $[P1 - 9H]^{9-}$ implies that the seven remaining deprotonated sites are distributed over the other two blocks, as shown in Figure 1C with $[B2 - 3H]^{3-}$ at *m/z* 606.5 and $[B3 - 4H]^{4-}$ at *m/z* 388.3. Additional fragments annotated in red in these CID spectra correspond to product ions obtained complementarily to individual blocks on alkoxyamine bond cleavages, as in the dissociation schemes shown as insets in Figure 1B,C. These multiblock fragments are particularly useful to determine block ranking in the initial chain (Figure S2).

For block sequencing in pseudo-MS$^3$ experiments, an appealing option to ensure best detectability of fragments is selection of 2– precursor ions, not only because their absolute abundance is higher than their 3– homologues but also because their fragments are expected to be distributed over at most two charge states (instead of three), therefore minimizing their signal dilution. This is a particularly important issue in the case of PPDEs because their CID proceeds via the cleavage of all bonds in phosphate groups, yielding four pairs of complementary products (Figure 2A; Table S1). This regular dissociation behavior is always observed for the first and the last blocks, regardless of their charge state (data not shown). In contrast, the variety of ion series produced in the CID of the inner blocks was observed to depend on their charge state. For the studied P1 triblock polymer, the CID of $[B2 - 3]^{3-}$ at *m/z* 606.5 yields the eight expected fragment families. Figure 2B shows that selecting multiple isotopes for the precursor ion permits to observe the whole isotopic pattern of product ions for safe determination of their charge state. However, in addition to these product ions, new fragment series are observed when activating $[B2 - 2]^{2-}$ at *m/z* 910.5 (Figure 2C). On the one hand, product ions containing the carbon-centered radical at the ω-end are also observed at −1 *m/z*, as shown with the *m/z* 672.1 dianion (dark brown) next to the regular $z_8^{2-}$ at *m/z* 672.6 (pale brown). On the other hand, all fragments holding the nitroxide α-termination are also detected with +1 *m/z* shift: this is evidenced by the peak at *m/z* 693.2 (dark green, Figure 2C) whose intensity is no longer consistent with the only $^{13}C$ contribution of the *m/z* 692.7 $d_6^{2-}$ fragment (pale green, Figure 2B). As supported by accurate mass measurements (Table S2), these additional ion series reveal that one H$^\bullet$ has been transferred from the ω- to the α-side of the inner blocks prior to their dissociation. These blocks are diradicals in which intramolecular radical addition could lead to cyclization (Scheme 2,

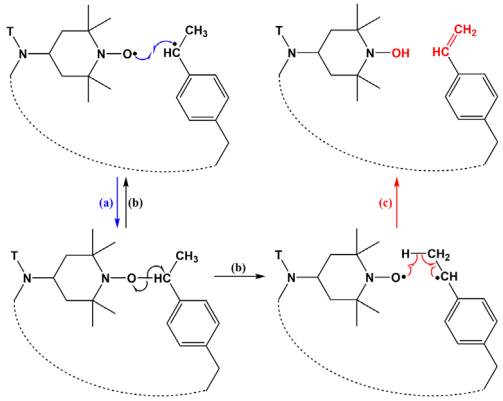

**SCHEME 2** Mechanism proposed to account for H$^\bullet$ transfer from the ω- to the α-group. Intramolecular addition of the two radical end groups of inner blocks (pathway a, in blue) would lead to a cyclic form, in which reopening via activated homolysis of the C–ON bond (pathway b, in black) could be followed by one H$^\bullet$ transfer (pathway c, in red) to produce close-shell species with a hydroxylamine α-group and one double bond at the ω-side. [Color figure can be viewed at wileyonlinelibrary.com]

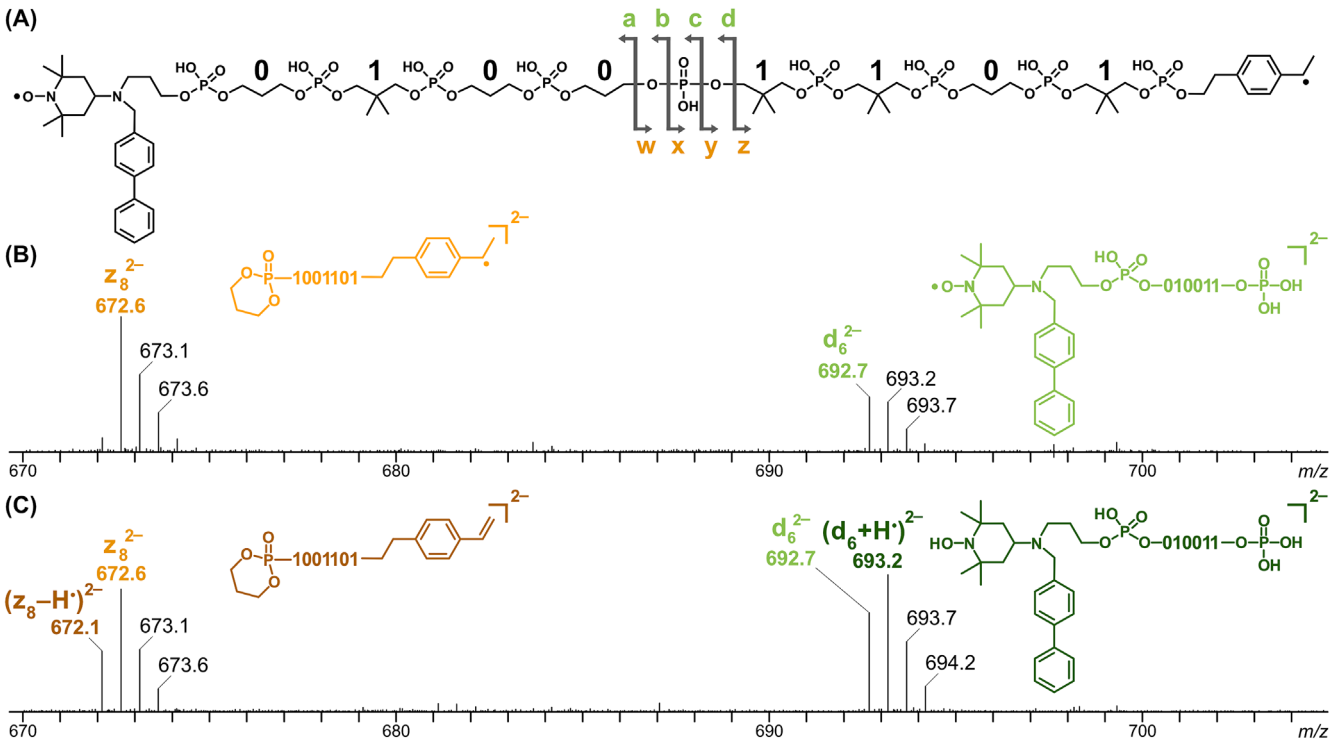


**FIGURE 2** (A) Structure of the 1822.5-Da inner block of P1 (B2 labeled with tag T5 in the α-group), also showing the nomenclature for the eight product ion series expected to form upon cleavage of all phosphate bonds in each repeating unit. Details of CID spectra recorded for (B) $[B2 - 3H]^{3-}$ at *m/z* 606.5 ($E_{coll}$: 13 eV) and (C) $[B2 - 2H]^{2-}$ at *m/z* 910.2 ($E_{coll}$: 27 eV). [Color figure can be viewed at wileyonlinelibrary.com]

step a). Cyclization via covalent bond formation is an exothermic process, as confirmed by energy calculations showing that the cyclic form is more stable by 52 kcal $mol^{-1}$ compared to its open diradical congener. As mentioned earlier, diradical blocks are produced in the interface of the mass spectrometer where the quite high pressure enables collisions to dissipate this excess energy and therefore prevent spontaneous reopening. Upon collisional activation, this cyclic conformation would open via homolysis of the C–ON bond to (i) restore the linear diradical form (Scheme 2, step b) or (ii) operate one $H^{\bullet}$ transfer according to the mechanism shown in red, leading to close-shell species with a hydroxylamine α-group and one double bond at the ω-side (Scheme 2, step c). Compared to the CID of diradical species, further cleavage of phosphate bonds in the close-shell chains would produce α-containing fragments with +1 *m/z* shift, as shown in the structure proposed for $(d_6 + H^{\bullet})^{2-}$ at *m/z* 693.2 in Figure 2C, as well as ω-containing fragments with −1 *m/z* shift, as shown in Figure 2C, with the structure assigned to $(z_8–H^{\bullet})^{2-}$ at *m/z* 672.1. The proposed cyclization process (and subsequent $H^{\bullet}$ transfer) would be less favored in $[B2 - 3H]^{3-}$ due to increasing repulsion forces between deprotonated sites. It would however occur to some extent, as revealed by the weak signal detected at *m/z* 672.1 in Figure 2B. In the field of synthetic polymers, IMS is well known for its ability to resolve linear and cyclic isomers,[31] so IMS-MS experiments have been performed to tentatively provide experimental evidence supporting the scenario proposed in Scheme 2.

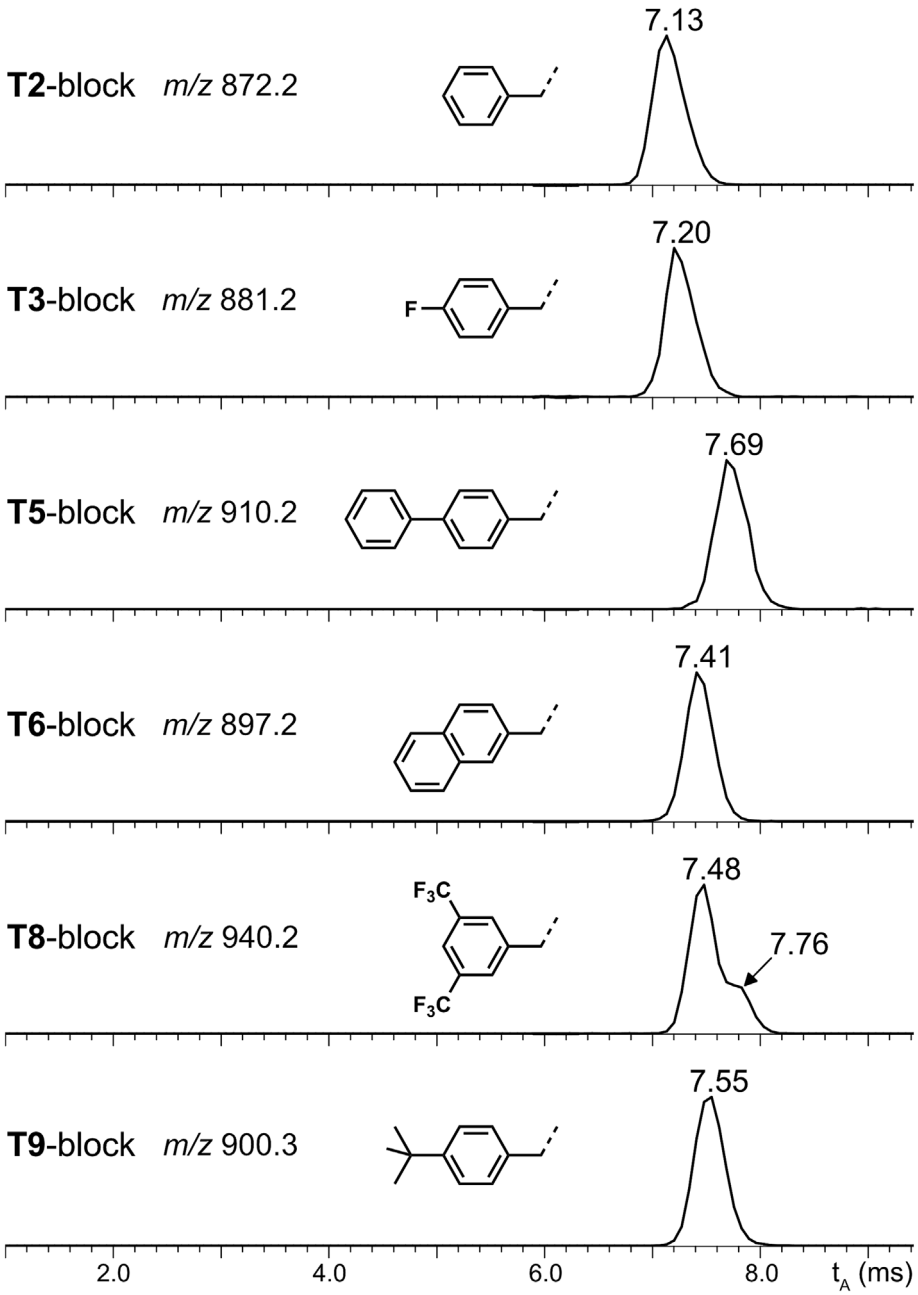


**FIGURE 3** Arrival time distributions (ATD) extracted for doubly deprotonated inner blocks sharing the same $0_4 1_4$ co-monomeric composition but labeled with a different Ti tag, shown as inset structures together with the monitored *m/z* values. These experiments were performed using WH (wave height) = 30 V and WV (wave velocity) = 550 m $s^{-1}$ in the TWIM (traveling wave ion mobility) cell.

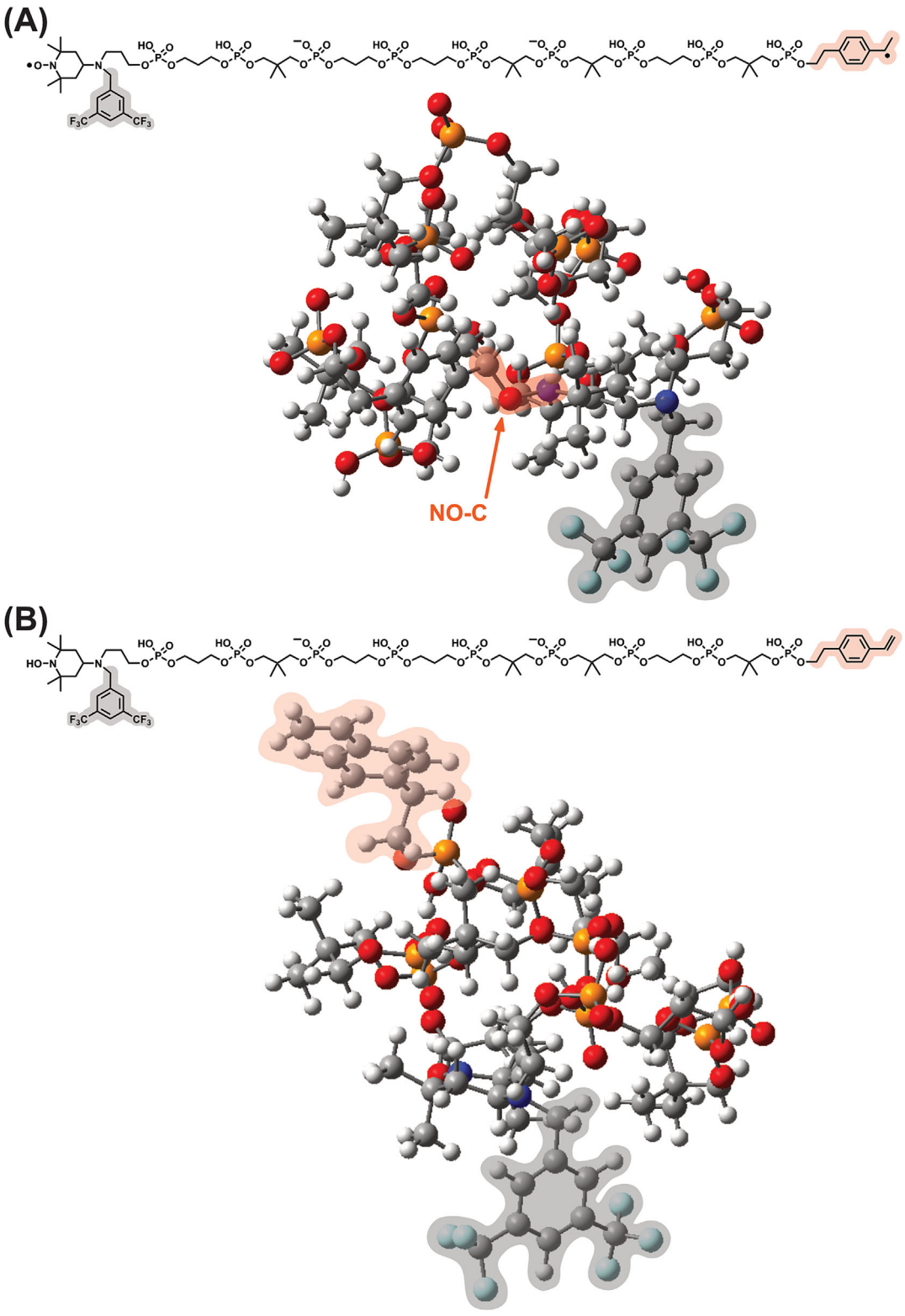


**FIGURE 4** Geometries obtained using molecular dynamics simulation for the $0_4 1_4$ inner block deprotonated at sites 3 and 6, with the tag T8 highlighted in grey and the ω-group in pale pink when (A) cyclized on addition of the carbon-centered radical in the ω-group onto the α-nitroxide or (B) in its open form after $H^{\bullet}$ transfer from ω to α, with linear structures shown on top. Data related to the diradical open form are shown in Figure S3. 3D models use atom-colored scaled sticks and balls: C, grey; H, white; N, blue; O, red; P, orange; F, pale blue. [Color figure can be viewed at wileyonlinelibrary.com]

### 3.2 | Evidence of cyclic/linear isomers using IMS

In all IMS-MS measurements, blocks were produced in the interface of the instrument upon in-source activation of their b-PPDE precursor and injected into the TWIM cell with no prior mass selection so that the same experimental conditions can be used with IMS calibration standards. Despite operating the TWIM cell in different conditions by varying the WH and WV, the ATD recorded for the doubly deprotonated inner block of P1 at *m/z* 910.5 always exhibits a single peak. This can mean either that the cyclic form of $[B2 - 2H]^{2-}$ does not exist or that the cyclic/open forms cannot be resolved using our instrument. In a recent study, we demonstrated that doubly charged inner blocks of b-PPDEs adopt a conformation where the tag, pointing out of the coil formed by the coded segment, strongly influences their IMS behavior.[32] Therefore, to investigate other species than the B2 block of P1 labeled with the T5 tag, five other triblock b-PPDEs with different tags labeling their inner block were considered (Table S3). This recent study also showed that the 0/1 sequence of the coded segment has no influence on arrival times measured using IMS as long as blocks have the same co-monomeric composition.[32] Therefore, for useful comparison, selected triblock polymers have the same $0_4 1_4$ composition for their B2 block. Figure 3 shows that ATDs extracted for each doubly charged species always exhibit a single major peak except when the inner block is labeled with the T8 tag, with a small shoulder clearly observed at the right-hand side of the main peak.

For comparing experimental data with CCS values calculated from 3D models in helium ($^{calc}CCS_{He}$, see below), standards with reference CCS in He were used to calibrate the TWIM cell. Doing so, $t_A$ measured for the two signals observed for the T8-block could be converted into $^{TW}CCS_{N2 \rightarrow He}$ values such as 330 ± 2 Å$^2$ for the first (more compact) species and 339 ± 2 Å$^2$ for the second conformation. These experimental data fit well with CCS values calculated from 3D models of this T8-block (Figure 4), with $^{calc}CCS_{He} = 327 \pm 3$ Å$^2$ for

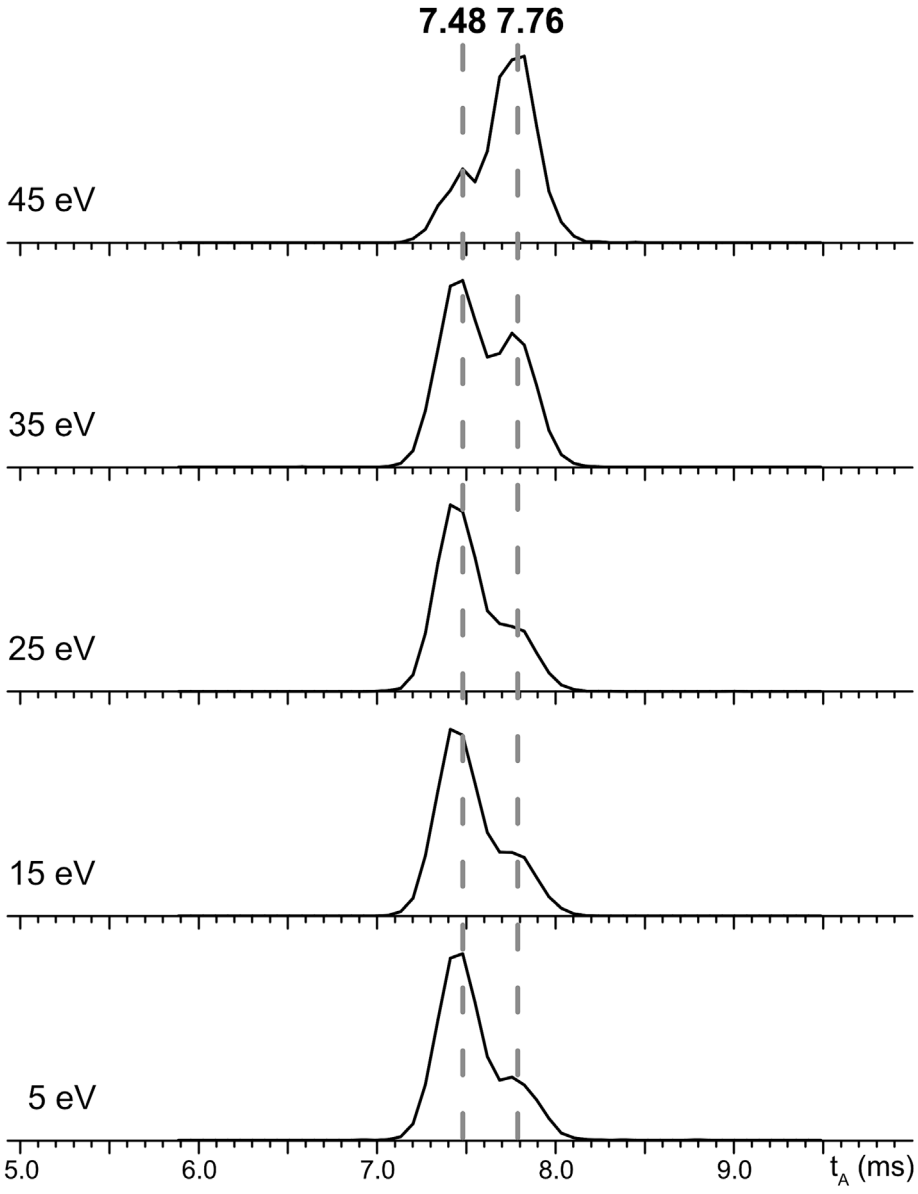


**FIGURE 5** Energy-resolved ATDs recorded for doubly deprotonated T8-block (*m/z* 940.2), with the cyclic isomer measured at $t_A = 7.48$ ms and its linear homologue at $t_A = 7.76$ ms.

the cyclic form (+0.9%) and $^{calc}CCS_{He} = 345 \pm 7$ Å$^2$ for the open form after H$^\bullet$ transfer (−1.8%). Of note, $^{calc}CCS_{He} = 340 \pm 3$ Å$^2$ was obtained for the diradical open form (Figure S3). The CCS difference experimentally observed between the two forms ($\Delta^{exp}CCS = 9$ Å$^2$) is lower than the predicted one ($\Delta^{calc}CCS = 18$ Å$^2$). Nevertheless, these findings permit to validate our assumption of two forms for this inner block, the cyclic isomer being slightly more compact than the open form, as commonly found for synthetic polymers analyzed either in the positive[33–36] or in the negative ion mode.[37] The same molecular modeling was performed for species labeled with alternative T-tags to rationalize the presence of only one peak in their ATDs. As shown using the T9-block, $^{calc}CCS_{He}$ values are 335 ± 4 Å$^2$ for the cyclic form (Figure S4A) and 343 ± 3 Å$^2$ for the close-shell open form obtained after H$^\bullet$ transfer (Figure S4B), slightly overestimating the $^{TW}CCS_{N2 \rightarrow He} = 335 \pm 2$ Å$^2$ value experimentally determined from IMS. More importantly, these calculations indicate that the $\Delta^{calc}CCS = 8$ Å$^2$ expected between these two forms of the T9-block is twice lower than the $\Delta^{calc}CCS = 18$ Å$^2$ predicted for the T8-block. This can fairly explain why the two forms of the T9-block cannot be distinguished in the quite low-resolution IMS device of our instrument.

Further evidence of the cyclization/reopening scenario proposed in Scheme 2 was obtained in energy-resolved IMS experiments, where the doubly deprotonated T8-block was gradually activated in the ion trap before being injected in the TWIM cell. Data in Figure 5 show that increasing the energy of the selected *m/z* 940.2 T8-block induces conversion of the cyclic isomer measured at $t_A = 7.48$ ms into the less-compact open form measured at $t_A = 7.76$ ms.

## 4 | CONCLUSIONS

Combining IMS experiments with molecular modeling enabled us to observe the cyclic form of inner blocks from which H$^\bullet$ transfer was suspected to produce close-shell species that dissociate into fragments with ±1 *m/z* shifts compared to CID products of diradical chains. With alkoxyamine bonds distributed along the chains to permit the release of small segments amenable to MS/MS sequencing, the diradical character of inner blocks is intrinsic to the design of b-PPDEs. Therefore, intramolecular radical addition cannot be avoided but may be prevented. Inspired by results observed for triply charged blocks, one option would be to increase the number of deprotonated sites per block so that cyclization would be disfavored by increased charge repulsions. This implies promoting higher charge states of b-PPDEs during ESI, which could be achieved by favoring supercharging effects,[38] using specific additives reported for their efficiency in the negative ion mode for structurally related species such as oligonucleotides.[39] An alternative strategy would be to decrease the length of coded segments, which should lead to more constraint (therefore less stable) structure upon cyclization. This could be done by distributing C–ON bonds between each group of four (instead of eight) repeating units and using an enhanced alphabet with each monomer coding for two digits instead of one,[40] to ensure similar storage density while using the same number of tags.

### 4.1 | Associated content

MS/MS of $[P1 - 7H]^{7-}$, determination of block ranking from MS/MS data, fragment series used for inner block sequencing, accurate mass measurement of selected sequencing fragments, list of b-PPDEs used in this study; 3D model of diradical open form of $[T8\text{-}B2 - 2H]^{2-}$, 3D models of cyclic/open forms of $[T9\text{-}B2 - 2H]^{2-}$.

### AUTHOR CONTRIBUTIONS

**ISAURE Sergent:** Investigation (MS, IMS and theoretical calculations). **Thibault Schutz:** Investigation (synthesis). **Jean-François Lutz:** Supervision of synthesis, funding acquisition. **Laurence Charles:** Conceptualization, supervision of MS and IMS, funding acquisition, writing, review, editing.

### ACKNOWLEDGMENTS

The authors thank the Agence Nationale de la Recherche for financial support (Project shapeNread, grant numbers: ANR-19-CE29-0015-01 and ANR-19-CE29-0015-02). Isaure Sergent thanks the Doctorate School *Sciences Chimiques* of Aix Marseille University for her PhD fellowship. Laurence Charles acknowledges support from Spectropole, the Analytical Facility of Aix-Marseille University, by granting a special access to the instruments purchased with European Funding (FEDER OBJ2142-3341). This work was also supported by the computing facilities of the *Centre Régional de Compétences en Modélisation Moléculaire* (CRCMM) of Aix Marseille University.

### CONFLICT OF INTEREST STATEMENT

The authors declare no competing financial interest.

### DATA AVAILABILITY STATEMENT

The data that support the findings of this study are available from the corresponding author upon reasonable request.

### ORCID

*Laurence Charles* https://orcid.org/0000-0003-3807-8375

### REFERENCES

1. Biemann K. Laying the groundwork for proteomics - mass spectrometry from 1958 to 1988. *Int J Mass Spectrom*. 2007; 259(1–3):1-7. doi:10.1016/j.ijms.2006.08.002
2. McLuckey SA, Vanberkel GJ, Glish GL. Tandem mass spectrometry of small, multiply charged oligonucleotides. *J Am Soc Mass Spectrom*. 1992;3(1):60-70. doi:10.1016/1044-0305(92)85019-g
3. Domon B, Costello CE. A systematic nomenclature for carbohydrate fragmentations in FAB-MS/MS spectra of glycoconjugates. *Glycoconj J*. 1988;5(4):397-409. doi:10.1007/bf01049915
4. Wesdemiotis C, Solak N, Polce MJ, Dabney DE, Chaicharoen K, Katzenmeyer BC. Fragmentation pathways of polymer ions. *Mass Spectrom Rev*. 2011;30(4):523-559. doi:10.1002/mas.20282

5. Jackson AT, Scrivens JH, Williams JP, Baker ES, Gidden J, Bowers MT. Microstructural and conformational studies of polyether copolymers. *Int J Mass Spectrom*. 2004;238(3):287-297. doi:10.1016/j.ijms.2004.09.025
6. Wesdemiotis C, Pingitore F, Polce MJ, et al. Characterization of a poly (fluorooxetane) and poly (fluorooxetane-co-THF) by MALDI mass spectrometry, size exclusion chromatography, and NMR spectroscopy. *Macromolecules*. 2006;39(24):8369-8378. doi:10.1021/ma0610414
7. Terrier P, Buchmann W, Desmazières B, Tortajada J. Block lengths and block sequence of linear triblock and glycerol derivative diblock copolyethers by electrospray ionization: Collision-induced dissociation mass spectrometry. *Anal Chem*. 2006;78(6):1801-1806. doi:10.1021/ac051308h
8. Girod M, Phan TNT, Charles L. Microstructural study of a nitroxide-mediated poly (ethylene oxide)/polystyrene block copolymer (PEO-b-PS) by electrospray tandem mass spectrometry. *J Am Soc Mass Spectrom*. 2008;19(8):1163-1175. doi:10.1016/j.jasms.2008.04.030
9. Fouquet T, Chendo C, Toniazzo V, Ruch D, Charles L. Collision-induced dissociation of synthetic polymers containing hydride groups: The case of poly (methylhydrosiloxane) homopolymers and poly (methylhydrosiloxane)-co-(dimethylsiloxane) copolymers. *Rapid Commun Mass Spectrom*. 2013;27(1):88-96. doi:10.1002/rcm.6432
10. Yol AM, Janoski J, Quirk RP, Wesdemiotis C. Sequence analysis of styrenic copolymers by tandem mass spectrometry. *Anal Chem*. 2014;86(19):9576-9582. doi:10.1021/ac5019815
11. Charles L, Cavallo G, Monnier V, Oswald L, Szweda R, Lutz J-F. MS/MS-assisted design of sequence-controlled synthetic polymers for improved reading of encoded information. *J Am Soc Mass Spectrom*. 2017;28(6):1149-1159. doi:10.1007/s13361-016-1543-5
12. Colquhoun H, Lutz J-F. Information-containing macromolecules. *Nat Chem*. 2014;6(6):455-456. doi:10.1038/nchem.1958
13. Roy RK, Meszynska A, Laure C, Charles L, Verchin C, Lutz J-F. Design and synthesis of digitally encoded polymers that can be decoded and erased. *Nat Commun*. 2015;6(1):7237. doi:10.1038/ncomms8237
14. Charles L. Tandem Mass Spectrometry Sequencing of Sequence-Controlled and Sequence-Defined Synthetic Polymers. In: Lutz J-F, ed. *Sequence-controlled polymers*. Wiley-VCH Verlag GmbH & Co; 2018:479-504. doi:10.1002/9783527806096.ch16
15. Laurent E, Amalian J-A, Schutz T, et al. Storing the portrait of Antoine de Lavoisier in a single macromolecule. *C R Chim*. 2021;24(2):69-76. doi:10.5802/crchim.72
16. Charles L, Lutz J-F. Design of abiological digital poly(phosphodiester)s. *Acc Chem Res*. 2021;54(7):1791-1800. doi:10.1021/acs.accounts.1c00038
17. Al Ouahabi A, Amalian J-A, Charles L, Lutz J-F. Mass spectrometry sequencing of long digital polymers facilitated by programmed inter-byte fragmentation. *Nat Commun*. 2017;8(1):967. doi:10.1038/s41467-017-01104-3
18. Amalian J-A, Al Ouahabi A, Cavallo G, et al. Controlling the structure of sequence-defined poly (phosphodiester)s for optimal MS/MS reading of digital information. *J Mass Spectrom*. 2017;52(11):788-798. doi:10.1002/jms.3947
19. Burel A, Carapito C, Lutz J-F, Charles L. MS-DECODER: Milliseconds sequencing of coded polymers. *Macromolecules*. 2017;50(20):8290-8296. doi:10.1021/acs.macromol.7b01737
20. Launay K, Amalian J-A, Laurent E, et al. Precise alkoxyamine design to enable automated tandem mass spectrometry sequencing of digital poly (phosphodiester)s. *Angew Chem Int Ed*. 2021;60(2):917-926. doi:10.1002/anie.202010171
21. Schutz T, Sergent I, Obeid G, et al. Conception and evaluation of a library of cleavable mass tags for digital polymers sequencing. *Angew Chem Int Ed*. 2023;62(45):e202310801. doi:10.1002/anie.202310801
22. Richardson K, Langridge D, Dixit SM, Ruotolo BT. An improved calibration approach for traveling wave ion mobility spectrometry: Robust, high-precision collision cross sections. *Anal Chem*. 2021;93(7):3542-3550. doi:10.1021/acs.analchem.0c04948
23. Calabrese V, Lavanant H, Rosu F, Gabelica V, Afonso C. Collision cross sections of phosphoric acid cluster anions in helium measured by drift tube ion mobility mass spectrometry. *J Am Soc Mass Spectrom*. 2020;31(4):969-981. doi:10.1021/jasms.0c00034
24. Sergent I, Adjieufack AI, Gaudel-Siri A, Siri D, Charles L. The IMSCal approach to determine collision cross section of multiply charged anions in traveling wave ion mobility spectrometry. *Int J Mass Spectrom*. 2023;492:117112. doi:10.1016/j.ijms.2023.117112
25. Pacholarz KJ, Barran PE. Distinguishing loss of structure from subunit dissociation for protein complexes with variable temperature ion mobility mass spectrometry. *Anal Chem*. 2015;87(12):6271-6279. doi:10.1021/acs.analchem.5b01063
26. Hoaglund CS, Liu YS, Ellington AD, Pagel M, Clemmer DE. Gas-phase DNA: Oligothymidine ion conformers. *J Am Chem Soc*. 1997;119(38):9051-9052. doi:10.1021/ja970652w
27. Stewart JJP. Optimization of parameters for semiempirical methods V: Modification of NDDO approximations and application to 70 elements. *J Mol Model*. 2007;13(12):1173-1213. doi:10.1007/s00894-007-0233-4
28. Frisch MJ, Trucks GW, Schlegel HB, et al. *Gaussian 16*. Gaussian Inc.; 2016.
29. Hess B, Kutzner C, van der Spoel D, Lindahl E. GROMACS 4: Algorithms for highly efficient, load-balanced, and scalable molecular simulation. *J Chem Theory Comput*. 2008;4(3):435-447. doi:10.1021/ct700301q
30. Larriba-Andaluz C, Hogan CJ. Collision cross section calculations for polyatomic ions considering rotating diatomic/linear gas molecules. *J Chem Phys*. 2014;141(19):194107. doi:10.1063/1.4901890
31. Charles L, Chendo C, Poyer S. Ion mobility spectrometry - mass spectrometry coupling for synthetic polymers. *Rapid Commun Mass Spectrom*. 2020;34(S2):e8624. doi:10.1002/rcm.8624
32. Sergent I, Schutz T, Oswald L, Obeid G, Lutz J-F, Charles L. Using nitroxides to model the ion mobility behavior of nitroxide-ended oligomers: A bottom-up approach to predict mobility separation. *J Am Soc Mass Spectrom*. 2024;35(3):534-541. doi:10.1021/jasms.3c00393
33. Hoskins JN, Trimpin S, Grayson SM. Architectural differentiation of linear and cyclic polymeric isomers by ion mobility spectrometry-mass spectrometry. *Macromolecules*. 2011;44(17):6915-6918. doi:10.1021/ma2012046
34. Kim K, Lee JW, Chang T, Kim HI. Characterization of polylactides with different stereoregularity using electrospray ionization ion mobility mass spectrometry. *J Am Soc Mass Spectrom*. 2014;25(10):1771-1779. doi:10.1007/s13361-014-0949-1
35. Alalwiat A, Grieshaber SE, Paik BA, Kiick KL, Jia XQ, Wesdemiotis C. Top-down mass spectrometry of hybrid materials with hydrophobic peptide and hydrophilic or hydrophobic polymer blocks. *Analyst*. 2015;140(22):7550-7564. doi:10.1039/c5an01600b
36. Chen X, Raab SA, Poe T, Clemmer DE, Larriba-Andaluz C. Determination of gas-phase ion structures of locally polar homopolymers through high-resolution ion mobility spectrometry-mass spectrometry. *J Am Soc Mass Spectrom*. 2019;30(6):905-918. doi:10.1007/s13361-019-02184-9
37. Scionti V, Katzenmeyer BC, Solak N, Li XP, Wesdemiotis C. Interfacing multistage mass spectrometry with liquid chromatography or ion mobility separation for synthetic polymer analysis. *Eur J Mass Spectrom*. 2012;18(2):113-137. doi:10.1255/ejms.1175
38. Iavarone AT, Jurchen JC, Williams ER. Supercharged protein and peptide lone formed by electrospray ionization. *Anal Chem*. 2001;73(7):1455-1460. doi:10.1021/ac001251t

39. Ghosh D, Rosu F, Gabelica V. Negative electrospray supercharging mechanisms of nucleic acid structures. *Anal Chem*. 2022;94(44): 15386-15394. doi:10.1021/acs.analchem.2c03187
40. Laurent E, Amalian J-A, Parmentier M, et al. High-capacity digital polymers: Storing images in single molecules. *Macromolecules*. 2020; 53(10):4022-4029. doi:10.1021/acs.macromol.0c00666

## SUPPORTING INFORMATION

Additional supporting information can be found online in the Supporting Information section at the end of this article.

**How to cite this article:** Sergent I, Schutz T, Lutz J-F, Charles L. Using ion mobility spectrometry to understand signal dilution during tandem mass spectrometry sequencing of digital polymers: Experimental evidence of intramolecular cyclization. *Rapid Commun Mass Spectrom*. 2024;38(17):e9852. doi:10.1002/rcm.9852